ORNL/CP-94844

CONF-9709116

REI Conference, Knoxville, TN, 9/97
(NIMB)

Investigation of Mn Implanted $LiNBO_3$ Applying Electron Paramagnetic Resonance Technique

A. Darwish and D. Ila
Alabama A&M University
Normal, AL

D. B. Poker and D. K. Hensley
Oak Ridge National Laboratory
Oak Ridge, TN

Prepared by the
Oak Ridge National Laboratory
Oak Ridge, Tennessee 37831
managed by
LOCKHEED MARTIN ENERGY RESEARCH CORP.
for the
U.S. DEPARTMENT OF ENERGY
under contract DE-AC05-96OR22464

October 1997

DISCLAIMER

Investigation of Mn Implanted $LiNBO_3$ Applying Electron Paramagnetic Resonance technique[1]

A. Darwish, Center for Nonlinear Optics and Materials, D. Ila* Center for Irradiation of Materials, Alabama A&M University, Normal, Al 35762; D. B. Poker and D. K. Hensley, Solid State Division, Oak Ridge National Laboratory, Oak Ridge, TN 37831

Abstract

The effect of ion implantation on the $LiNbO_3$ crystal is studied using electron paramagnetic resonance spectroscopy (EPR). EPR measurements on these crystals were performed as a function of ion species Mn and Fe and fluence at room temperature. Also the effect of the laser illumination on the EPR signal was determined by illuminating the crystal in situ and measuring the decay and growth of the EPR signal. $LiNbO_3:Mn^{2+}$ at a depth of approximately 200 nm was formed by implantation of 2.5×10^{14} Mn/cm^2 and 1×10^{17} Mn/cm^2 at 2 MeV. The implanted samples were compared with bulk doped crystals. It was found that the decay and growth of Mn EPR for the implanted crystal is very small compared with the bulk doped $LiNbO_3$:Mn crystal. This was found to be primarily due to the spin concentration on the crystals. On the other, hand the decay time of the high fluence is about 40% slower than the decay of the low fluence implanted crystal.

***Corresponding author. FAX +1-205-851-5868, email:ila@cim.aamu.edu**

Introduction

$LiNbO_3$ is a ferroelectric crystal with a variety of applications. Dopants play an important role in developing favorable properties for optical purposes. Transition metals (e.g. Fe, Mn) increase the photorefractive sensitivity. The properties and applications of lithium niobate have been widely studied. The high level of interest in lithium niobate is due to its combination of useful dielectric, elastic and opto-electronic properties. This, together with the ready growth of large high-quality single

crystal from the melt, has recently increased even further as its electro-optic devices use has led to optical switching speeds as fast as 50 ps. In consequence, high speed switches, modulators, waveguide arrays, filters and polarization converts have been built based on lithium niobate.

The electron paramagnetic resonance measurements can provide critical information about structural and transport properties of the implanted samples as they give information on the spin mobility and degree of localization. EPR also can determine the effect of the laser illumination on the spin concentration and the charge carrier on the crystals. Also, it can identify the ions that participate in the processes of the charge transfer.

We have reported EPR investigation of $LiNbO_3$: Fe^{3+}:Mn^{4+} and the effect of the irradiation, which produced a new center [1]. Although there have been many studies of impurity states in $LiNbO_3$ by EPR[2-4], the analysis of Fe impurity is especially of importance because this impurity appears to be responsible for optical refractive index damage and phase holographic storage in $LiNbO_3$. Identification of the specific impurities and other defects that participate in the photorefractive effect is an important goal since this information will allow a material to be optimized for any particular set of applications.

Experimental

X-cut single crystals of $LiNbO_3$, EPI polished were implanted by 2.0 MeV Mn at room temperature at two fluences of 2.5×10^{14} /cm^2 and 1×10^{17}/cm^2. The Electron Paramagnetic Resonance was taken using Bruker X-band 300ESP spectrometer. The modulation frequency was 100 kHz and the microwave frequency was 9.3 GHz. The sample was placed in an optical cavity to utilize the usage of the laser while acquiring the spectrum and also to facilitate the selective illumination of the sample without illuminating the walls of the cavity. This gives unambiguous evidence of any photoinduced charge transfer occurring in the sample. DPPH with g value 2.0036 was taken as a g-marker and a

reference for the calculation of the spin concentration. A HeNe laser with 35mW power was used as sources of light.

Structure of $LiNbO_3$ and possible site for Mn^{2+}

The structure of $LiNbO_3$ is related to that of the ABO3 perovskites [5]. The structure is different, however, essentially because Li^+ and Nb^{5+} have nearly identical ionic radii, unlike the general perovskites A and B ions. In ferroelectric LiNbO3 the environments of Li^+ and Nb^{+5} are similar. Both ions are surrounded by a distorted octahedron of six O^{2-} ions. Because of the similarity of Li and Nb sites, and since the Nb^{+5}-O^{2-} bond is stronger than the Li^+-O^{-2} one, $LiNbO_3$ has a tendency to non-stoichiometry with Li/Nb < 1. Such crystals therefore have a very high concentration of intrinsic defects. This flexibility of the structure can also explain why $LiNbO_3$ can tolerate high concentration of extrinsic defects.

Results and Discussion

Naturally the difference between low-spin Fe (III) and Mn (II) is of interest. The smaller anisotropy found for the Mn (II) systems is in marked contrast to that of the Fe (III) systems. This results in part from the smaller spin-orbit constant for Mn (II) compared with the one for Fe (III). The values reported here reflect fairly weak tetragonal fields. Therefore, the binding of the coordinating OH- legend to Mn (II) must be relatively weak. In the latter case, the need for some involvement of excited state corrections to the g-factors must also reflect a smaller cubic part of the crystal field. The EPR signals in the figures are lines related to Mn^{2+} (s=5/2). This assignment is based on the fact that the sextet-lines are due to hyperfine interaction of the d electrons of Mn with the s=5/2, ^{55}Mn nucleus.

One strong set of sextets is observed, at θ =0° and 90°, the other weak two are overlapping with the Fe broad line which decreases the resolution of the hyperfine structure splitting. It is clear that the crystal is inherited with Fe^{3+}, which is playing the main role in the photorefractive processes in these crystals.

There are three possible sites for paramagnetic impurities in $LiNbO_3$, a Li site, a Nb site and a structural vacancy. Arguments have been advanced which favor both the Li and Nb sites as possible candidates for the Mn^{2+} and Fe^{3+} impurities. The EPR studies of Cr^{3+} in $LiNbO_3$ have shown that both the Li and Nb sites are possible candidates for the Cr^{3+} impurity.

The spectrum for the $LiNbO_3$: Mn^{2+} for high fluence is shown in figures 1 and 2 at $\theta = 0$, and 90, where θ is the angle between the c-axis and the magnetic field. To interpret the spectrum, we use an axially symmetric spin Hamiltonian of the form [6,7]

$$H=g\beta H\cdot S+B^0_2 O^0_2 + B^0_4 O^0_4 + B^3_4 O^3_4 + (B^3_4 O^3_4)^* + A S\cdot I$$

In this expression

$$O^0_2 = 3S^2_Z - S(S+1),$$

$$O^0_4 = 3\,5\, S^4_Z - 30S(S+!)\, S^2_Z + 25\, S^2_Z - 6S(S+1),$$

$$O^3_4 = \tfrac{1}{4}\,[S^Z (S^3_+ + S^3_-) + (S^3_+ + S^3_-) S_Z]$$

and the coordination system is chosen so that the Z-axis lies along the [111] or C axis of the crystal. For completeness, the hyperfine interaction term has been included in the Hamiltonian.

At $\theta = 0$, the energy eigenvalues are given by [6]

$$E(\pm 5/2) = \pm g_{\parallel}\, \beta H + B^0_2 + 90\, B^0_4 + \{[\pm(3/2)\, g_{\parallel}\, \beta H + 9\, B^0_2 - 30\, B^0_4]^2 + 90\, |B^3_{4\parallel}|^2\}^{1/2},$$

$$E(\pm 3/2) = \pm 3/2\, g_{\parallel}\, \beta H - 2B^0_2 - 180\, B^0_4,$$

$$E(\pm 1/2) = \pm g_{\parallel}\, \beta H + B^0_2 + 90\, B^0_4 - \{[\pm(3/2)\, g_{\parallel}\, \beta H + 9\, B^0_2 - 30\, B^0_4]^2 + 90\, |B^3_{4\parallel}|^2\}^{1/2},$$

where the eigenvalues refer to the high field limit. From the position of the transitions and the energy expression noted above, values for g, B^0_2, B^0_4, and $|B^3_{4\parallel}|$ can be determined. This analysis gives

$B^0_2 = 235$, $B^0_4 = -0.05$, and $|B^3_{4\parallel}| = 10$ (all in gauss) and $g = 1.9987$.

To interpret the EPR for the $LiNbO_3$: Fe crystal, Fe^{3+} ($S = 5/2$) was found in an axially symmetric site and is described by the spin Hamiltonian [7]

$$H=g\beta H\bullet S+B^0_2\,O^0_2+B^0_4\,O^0_4+B^3_4\,O^3_4$$

This Hamiltonian is different from the Mn^{2+} in the last term which we ignored for the axially symmetric site.

The crystal field parameters at room temperature were found to be

$B^0_2 = 560$ G, $B^0_4 = -0.902$ G and $B^3_4 = 11$ G

Some lines as pointed out are due to Fe^{3+}. These lines are sharp and even more intense than the $1/2 \Leftrightarrow -1/2$ transition of Mn^2. Even though this is the case, still the Fe lines are very sensitive to the laser illumination as shown in Figure 5.

Decay and growth of the EPR signals under laser illumination

As shown in Figure 5, there is much difference in the response of the ions involved in the decay processes. The different times are due first to the amount of ions available to share in the processes, and also to the location of the ions in the crystal structure, i.e., if it is either in the Li, Nb, or interstitial site. If the electronic radii are smaller than the Li or the Nb ions, then there is a high possibility that replacement processes will occur during crystal growth. If the radii are larger than the ions, then the possibility is less and the interstitial site will be higher, even though some ions will squeeze themselves into some of the legend sites. Having a crystal with relatively high-inherited ions will lead to actually lowering the percentage of the dopants in the crystal. Figure 5 shows that the decay of the EPR signal from Fe^{3+} is larger on the high fluence crystal than on the lower fluence one by 40%. It was found that the decay and growth of Mn EPR for the implanted crystal are very small compared with that of the bulk doped $LiNbO_3$: Mn crystal. This was found to be primarily due to the spin concentration on the crystals. On the other hand, the decay time of the high fluence is about 40% slower than the decay of the low fluence implanted crystal.. This is due to the fact that the process of the charge transfer from Fe^{3+} to Fe^{2+}/ Fe^{4+} is reversible. By turning the laser off one can see that the EPR signal gains back its strength in relatively the same time. On the other hand, the process of the charge transfer from Mn^{2+}

was not strong enough to be measured. This is due to the overlapping of the Fe line and the broad cubic Fe line, which decreased the resolution of the Mn lines.

For the spin concentration measurements were done by comparing the integrated intensity of the EPR signal with that of a known standard DPPH-diphenyl picryl-haydrazyl using a standard sample DPPH to be used in the measurements on the double cavity and to relate the two EPR signals to each other.

$$S_x = P/R \qquad (1)$$

as $P = S_{std}\, A_x\, R_x\, Scan_x^2\, G_{std}\, M_{std}\, (g_{std})^2\, S(S+1)_{std}$ and

$R = A_{std}\, R_{std}\, Scan_{std}^2\, G_x\, M_x\, g_x^2\, s(s+1)_x$

where S_{std} is the concentration of the standard, A is the area under the EPR curve or the integration of the absorption signal, G is the gain, M is the modulation amplitude, s is the spin value, Scan is the amplitude of the magnetic field sweep, R is the multiplicity, and g is the g-value.

Conclusions:

From the integrated intensity, the analysis given using equation 1 yields spin concentration of 2 $10^{18}/cm^3$ for the of 2.5 10^{14} $/cm^2$ fluence and $10^{22}/cm^3$ for 10^{17} $/cm^2$ fluence. The higher number of the spin concentration for the high fluence crystal accounted for the inherited Fe impurities on the crystal as well as the implanted Mn ions. The difference on the decay time for Fe in both crystals with high and low fluence is found to be due to the long spin lattice relaxation time for Fe^{3+} at room temperature and the structure of the $LiNbO_3$ crystal.. The spin concentration in these crystals was measured and the effect of the inherited Fe ions was studied.

Acknowledgments:

Research sponsored by the Center for Nonlinear Optics and Materials and the Center for Irradiation of Materials of Alabama A&M University and by the Division of Materials Science, U.S.

Department of Energy, under contract DE-AAC05-96OR22464 with Lockheed Martin Energy Research Corp.

References:

1. A. Darwish, D. McMillen, T. Hudson, and P. Banarjee, "Investigations of the charge transfer and the photosensitivity in single and double doped $LiNbO_3$ single crystals; an optical-electron paramagnetic resonance study (Part I)", ,J . Opt. Eng., Tech Digest, Vol. 2362, 29-31, 1997.
2. A.A. Mirzakhanyan, "The splitting in zero field of ground state levels of the Ni^{2+} ion in $LiNbO_3$," *Sov. Phys. Solid State* **23**, 8, 1981.
3. F. Jermann and J. Otten ,"Light induced charge transport in $LiNbO_3$:Fe at high light intensities," *J. Opt. Soc. Am. B*, Vol. **10**,11,2085-2092, 1993.
4. H. Towner and H. Story, "EPR studies of crystal field parameters in Fe^{3+}:$LiNbO_3$", *The J. of Chem. Phys.*, Vol. 56, 7, 1972.
5. L.E. Halliburton and C. Chen, "ESR and optical point defects in Lithium Niobate," *Nuc. Inst. And Methods in Phys. Res.*, B1, 344-347, 1984.
6. P. Gunter and J.P. Hunignard, *Photorefractive Materials and Their Applications I and II* , Springer-Verlag, Heidelberg, 1988, 1989.
7. F. Huixinan, W. Jinke, W. Huafu, and X. Yunxia, "EPR studies of Fe in Mg-Doped $LiNbO_3$ crystals", *J. Phys. Cem. Solids* Vol. **51**, No. 5, 397-400, 1990.

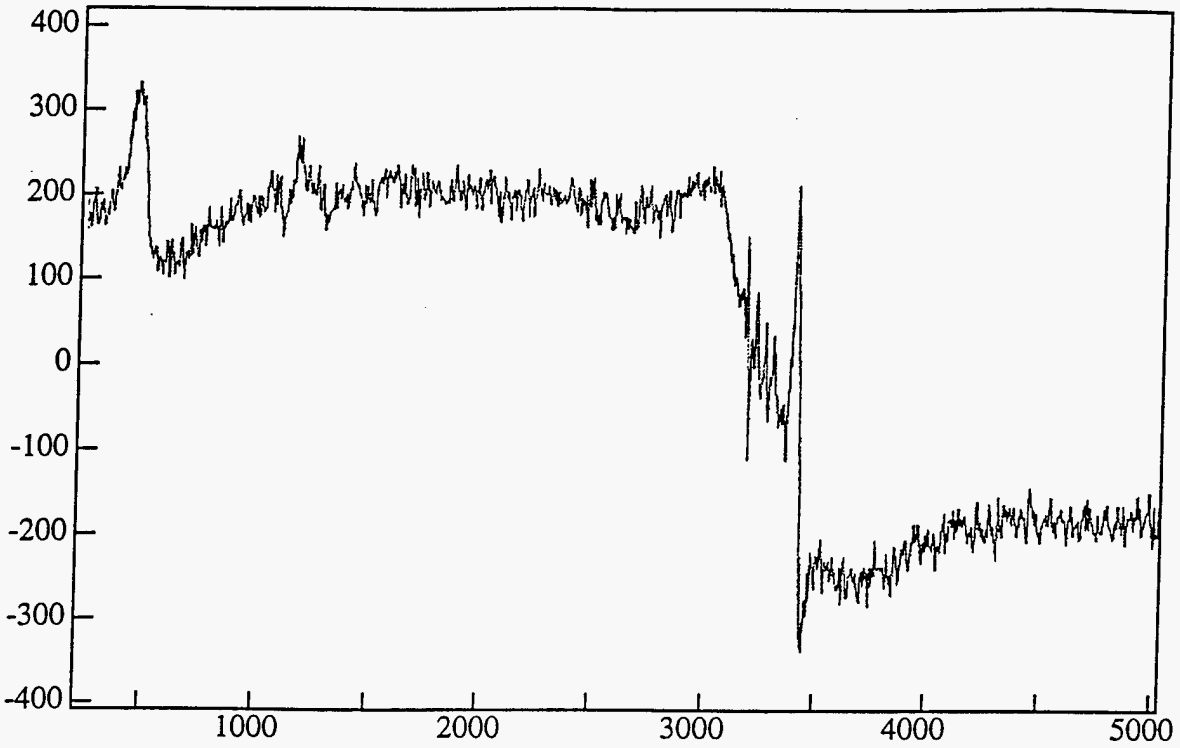

Figure 1. EPR spectrum for $LiNbO_3:Mn^{2+}$ high fluence z-axis perpendicular to the magnetic field.

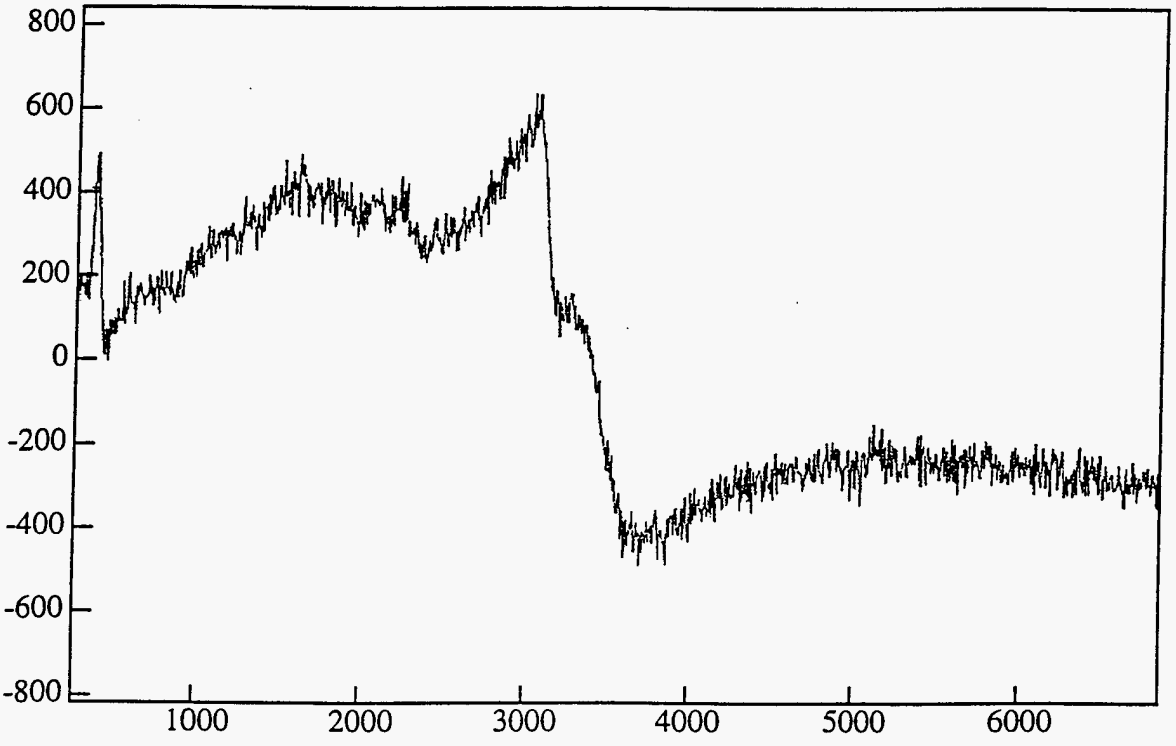

Figure 2. EPR spectrum for $LiNbO_3:Mn^{2+}$ "high fluence" z-axis parallel to the magnetic field.

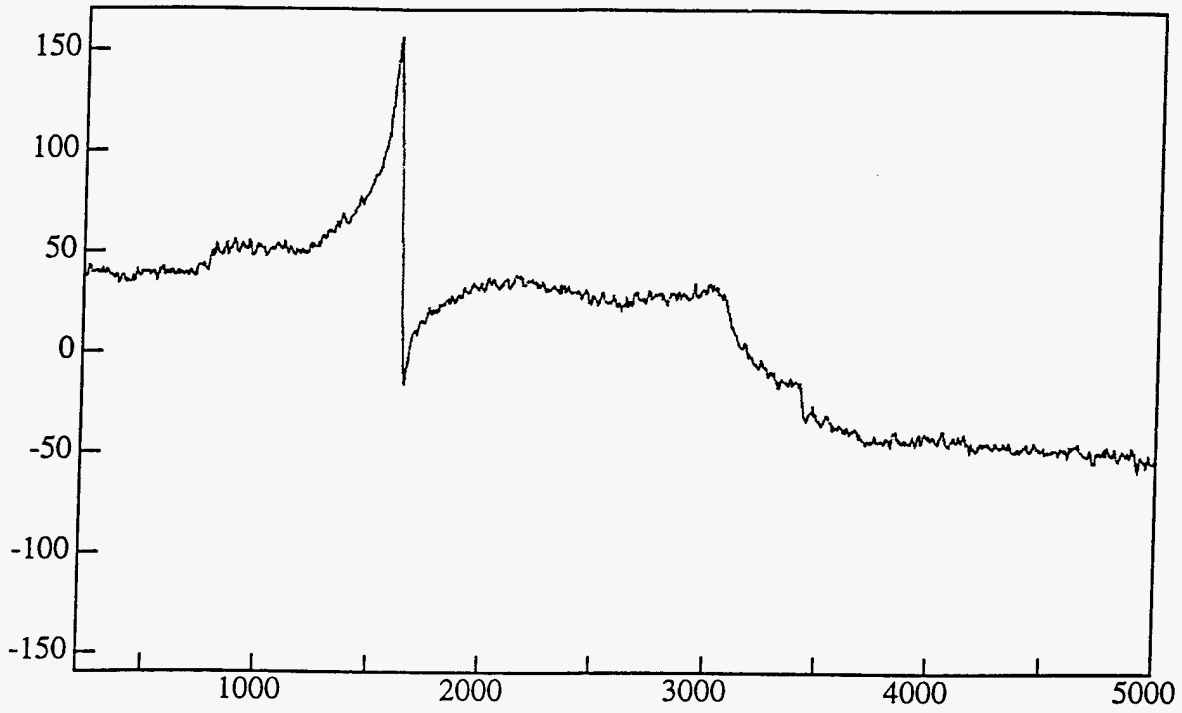

Figure 3. EPR spectrum for $LiNbO_3:Mn^{2+}$ low fluence z-axis perpendicular to the magnetic field.

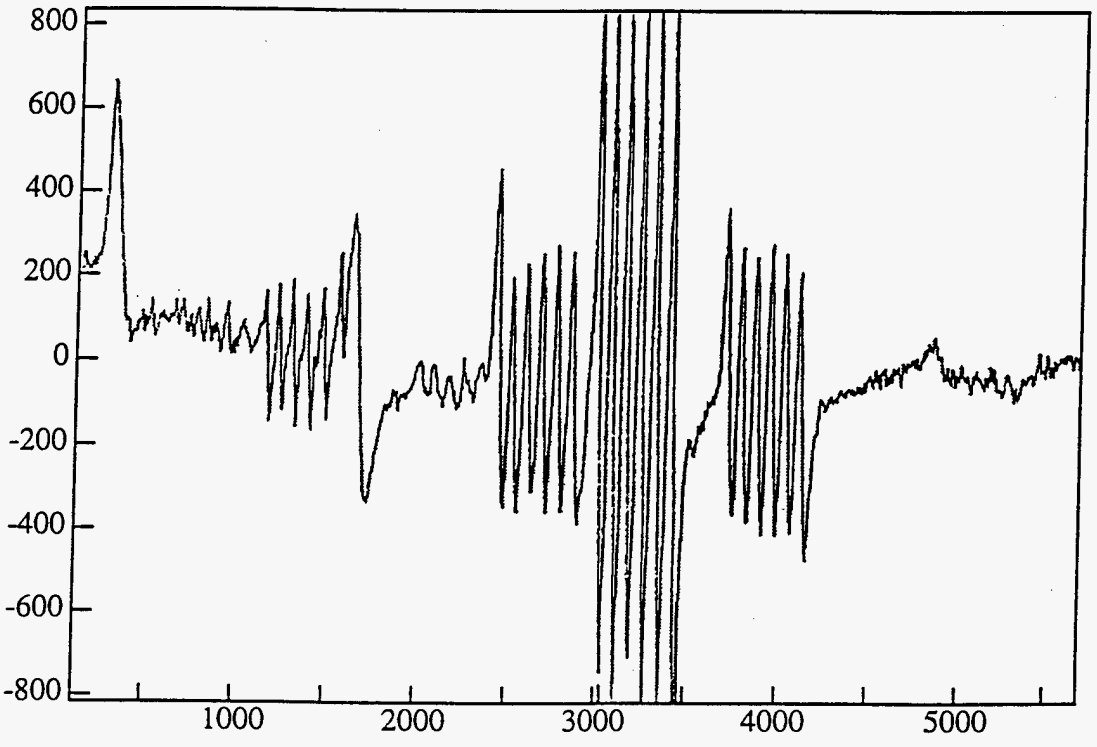

Figure 4. EPR spectrum for $LiNbO_3:Mn^{2+}$ Fe^3 doped crystal z-axis perpendicular to the magnetic field.

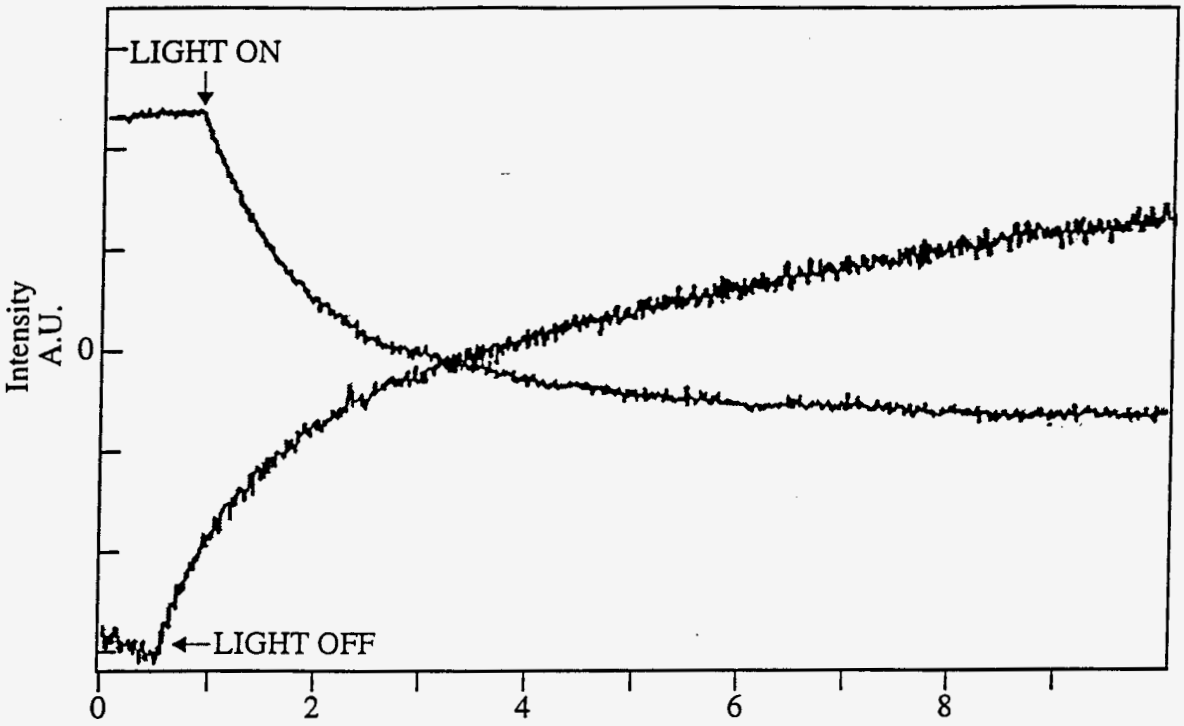

Figure 5. Decay and growth of the EPR Fe^{3+} signal in the "low fluence" crystal.

Report Number (14) ORNL/CP--94844
CONF-9709116--

Publ. Date (11) 1997 10
Sponsor Code (18) DOE/ER, XF
UC Category (19) UC-400, DOE/ER

DOE